Volume 10, Issue 1, 2020, 4876 - 4892 ISSN 2069-5837

Biointerface Research in Applied Chemistry

www.BiointerfaceResearch.com

https://doi.org/10.33263/BRIAC101.876892

Original Research Article **Open Access Journal**

Received: 06.11.2019 / Revised: 21.12.2019 / Accepted: 22.12.2019 / Published on-line: 29.12.2019

Investigating the behaviors of corticosterone hormone in different solvents by using DFT calculations and experimental data

Davide Romani[1], Silvia Antonia Brandán [2, *]

[1]SST, Servicio sanitario della Toscana, Azienda USL 9 di Grosseto, Via Cimabue, 109, 58100 Grosseto, Italia.
[2]Cátedra de Química General, Instituto de Química Inorgánica, Facultad de Bioquímica. Química y Farmacia, Universidad Nacional de Tucumán, Ayacucho 471, (4000) San Miguel de Tucumán, Tucumán, Argentina

*corresponding author e-mail address: ***sbrandan@fbqf.unt.edu.ar*** | Scopus ID 6602262428

ABSTRACT

In this work, structural, electronic, topological and vibrational properties of corticosterone hormone have been investigated in aqueous, ethanol and methanol solutions by using DFT calculations and experimental available infrared, attenuated total reflectance (ATR), Raman and Ultraviolet spectra. The properties predicted in the different solvents at the B3LYP/6-31G* level of theory were compared with those obtained in gas phase and, with others reported for steroids species at the same level of theory. The universal solvation model has evidenced higher solvation energy for corticosterone in aqueous solution and a higher value in methanol, as compared with the corresponding values to equilenin, equilin and estrone steroids in the same medium. Higher Mulliken charges on O atoms of C=O group of side chain are observed in the three solvents than the corresponding to C=O group of ring A while the MK charges on O atoms of OH group of ring C present higher values than the corresponding to O atoms of OH group of side chain. The natural bond orbital (NBO) studies have revealed a low stability of corticosterone in aqueous solution, as compared with the values in ethanol and methanol solutions, in total agreement with the higher solvation energy and dipole moment in this medium. On the other hand, the atoms in molecules (AIM) analyses support the lower stabilities of corticosterone in the three solutions because only five H bonds interactions different from of gas phase where six interactions are observed. The gap values suggests that corticosterone is most reactive in aqueous solution than the other solutions, as supported by the low stability and higher solvation energy and dipole moment values in this medium. This study shows clearly that the steroid species most reactive, equilenin and corticosterone, are characterized by a high global electrophilicity index value and low nucleophilicity index. Reasonable correlations in the predicted IR, Raman and UV spectra were observed, as compared with the corresponding experimental ones. Additionally, the complete vibrational assignments of all 159-vibration modes of corticosterone together with the harmonic force fields and force constants in the different media are for the first time presented.

Keywords: *Corticosterone; Force fields; Vibrational analysis; DFT calculations; Molecular structure.*

1. INTRODUCTION

The combination of theoretical density functional theory (DFT) calculations by using hybrid B3LYP methods with different experimental spectroscopic techniques is a very good methodology to elucidate reliably and effectively structural, electronic, topological and vibrational properties of diverse compounds [1-15]. The use of this methodology in species containing fused rings such as alkaloids, antihistaminic agents and species steroids, has allowed the optimizations of theoretical structures and the determination of their properties [1-15] while the complete assignments of all bands observed in the experimental infrared and Raman spectra were possible by using the normal internal coordinates, the SQMFF methodology and the Molvib program [16-18]. Now, the identifications of cocaine, heroin, morphine and scopolamine alkaloids [1,3-5,7], of antihistaminic agents promethazine [8] and of equilenin, equilin and estrone steroids [9] can be easily carried out in all media by using vibrational spectroscopy. For instance, in cocaine and scopolamine only two fused rings of five and six members' can be seen, in promethazine three six members`s rings are fused [8], in equilenin, equilin and estrone steroids four fused rings named A, B, C and D can be observed [9] while in morphine and heroin five fused rings [1, 3-5,7]. In the studies on steroids species, the differences in the dipole moment and volume values predicted for equilin could probably be explained from a structural point of view due to e unsaturated C=C bond in the B ring, as compared with estrone and equilenin [9] while the aromatic naphthalene core of both A and B rings of equilenin support the differences with the other ones, as was evidenced experimental and theoretically by the mapped molecular electrostatic potential (MEP) surfaces. The natural bond orbital (NBO) studies support the higher stability of equilin, in relation to equilenin and estrone while the atoms in molecules (AIM) analyses reveal the higher stability for estrone. Moreover, equilenin is the most reactive species probably due to its higher global electrophilicity while the higher global nucleophilicty values are observed for equilin and estrone. In this work, the structures and properties of corticosterone, a glucocorticoid hormone (GC), were studied employing the same methodology that for those species with fused rings [1-9] because, as can be seen in **Scheme 1** the structure of corticosterone has four A, B, C and D rings. The IUPAC name of corticosterone is (11β)-

11,21-dihydroxypregn-4-ene-3,20-dione although it is also known as 11β,21-dihydroxyprogesterone or simply as 17-deoxycortisol [19-44].

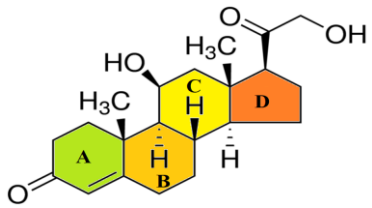

Scheme 1. Structure of corticosterone with definitions of four rings.

The adrenal gland produces this hormone with anti-inflammatory and immunosuppressive properties [20,21,23,27,30-32,35-37,39-44]. So far, there are a lot of articles related to structural, chemical and biological studies on glucocorticoids, from experimental studies by using spectroscopic and electrochemical techniques up to different theoretical studies [19-44] because these species present dual regulation effects on the immune function which are strongly dependent on the concentration. Thus, experimental structures of corticosterone .and their derivatives were already reported [19,24,25,29] together with other theoretical studies on structure, descriptors and reactivity [22,26,37]. Additional studies on temperature effects in low-frequency Raman spectra and terahertz adsorption and Raman scattering were also reported for corticosteroid and mineralocorticoid hormones [33,34], respectively but, the complete vibrational assignments of corticosterone in the different media by using SQMFF methodology were no reported yet. In this context, the aims of the work are the determination of most stable structure of corticosterone in gas phase and in aqueous, ethanol and methanol solutions in order to know its structural, electronic, topological and vibrational properties in those media and, then to perform the complete vibrational assignment of its infrared and Raman spectra by using the corresponding force fields. Here, hybrid B3LYP/6-31G* calculations were employed in the determination of all properties of corticosterone in the different media [45,46]. These results for corticosterone were compared with the reported for equilenin, equilin and estrone steroids in gas phase by using the same method. Here, the study of frontier orbitals and descriptors in all media are fundamental to explain the differences among them because the four steroids have four fused rings [9]. The idea is that these comparisons can allow the elucidation of mechanisms of action of steroid hormones and their interaction with different biological species.

2. MATERIALS AND METHODS

The original corticosterone structure was optimized in gas phase and aqueous, ethanol and methanol solutions with the Revision A.02 of Gaussian program [47] and the hybrid B3LYP/6-31G* method [45,46]. The corticosterone structure is presented in **Figure 1** with the atoms labelling and the definitions of four rings in different colours, as presented in scheme 1. The initial structure of corticosterone was modeled with the *GaussView* program [48] in accordance with the experimental structure reported [19,24,25,29]. The optimizations of corticosterone in the three solutions were performed taking into account the solvent effects with the integral equation formalism variant polarised continuum method (IEFPCM) while the universal solvation model was used to compute the solvation energies [49-51]. Later, the optimized geometrical parameters in the three media were used to calculate the atomic charges, molecular electrostatic potential, bond orders, frontier orbitals and topological properties by using Merz-Kollman charges and the NBO and AIM2000 programs [52-54] while the volume variations were computed with the Moldraw program [55]. The harmonic force fields in the three media were calculated with the scaled quantum mechanical force field (SQMFF) and the Molvib program by using the normal internal coordinates and transferable scaling factors [16-18]. After that, the vibrational analyses of all bands observed in the experimental available infrared, attenuated total reflectance (ATR) and Raman spectra [56] were carried out considering potential energy distribution (PED) contributions ≥ 10% and the corresponding force fields. Known equations were used to transform Raman activities in intensities [57,58]. The ultraviolet spectra of corticosterone in the three solutions were predicted by using the time-dependent DFT calculations (TD-DFT) and the hybrid B3LYP/6-31G* [18]. Reasonable correlations were found among the predicted IR, Raman and UV spectra with the corresponding experimental ones [56]. The calculations of gap values [54] and some descriptors were performed, as suggested by Parr and Pearson [59-68], because the prediction of reactivities and behaviours in the three media are of interest for this hormone with anti-inflammatory and immunosuppressive properties [20,21,23,27,30-32,35-37,39-44].

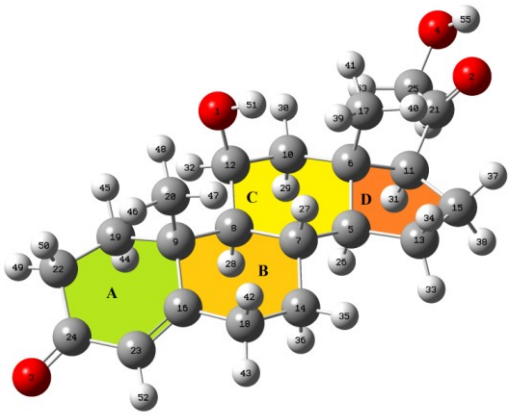

Figure 1. Molecular theoretical structures of corticosterone showing the four rings in different colours.

3. RESULTS

3.1. Geometrical parameters in the three media.

Some calculated properties for corticosterone in the different media by using the B3LYP/6-31G* method can be seen in **Table 1**. The total energies expressed in Hartrees were corrected by zero point vibrational energy (ZPVE) while the dipole moment and volume values are presented as function of permittivity values of different media. Both properties increase with the increase of permittivity presenting the higher values in aqueous solution while the volume value in ethanol is slightly higher than the corresponding in methanol. **Figure 2** shows that

the orientations, magnitudes and directions of dipole moment vectors in the four media are slightly different among them, especially in the three solutions, as compared with the value in gas phase.

Table 1. Calculated total energies (*E*) and dipole moments (μ) and volumes (V) of corticosterone in different media by using the B3LYP/6-31G* method.

B3LYP/6-31G* Method					
Medium	E (Hartrees)	ZPVE (Hartrees)	μ (D)	V (Å^3)	ε
Gas phase	-1119.1687	-1118.6840	3.54	382.2	1.00
Ethanol	-1119.2061	-1118.7224	4.53	383.4	24.85
Methanol	-1119.2071	-1118.6827	4.63	383.3	32.61
Aqueous	-1119.1975	-1118.7130	4.72	383.7	78.35

.

The solvation energies for corticosterone in the different media by using the B3LYP/6-31G* method are given in **Table 2** compared with the values calculated here for equilenin, equilin and estrone steroids in methanol solution. In this work, the $\Delta G_{un}^{\#}$ values for corticosterone in the three solvents were uncorrected by ZPVE because of the difference between the values in methanol solution and gas phase, -1118.6827 and -1118.6840 Hartrees is 3.41 kJ/mol, a value completely different from those calculated in ethanol (100.72 kJ/mol) and aqueous solution (76.07 kJ/mol). For this reason, in the calculations of $\Delta G_{un}^{\#}$ only the E values taken from first column of Table 1were considered. In the same way, the values for the other steroids were uncorrected by ZPVE. These results predict higher solvation energy for corticosterone in water evidencing probably a higher solubility and justifying, this way, the higher dipole moment value in this medium. On the other hand, higher volume expansion is also predicted for corticosterone in aqueous solution due to its high dipole moment value in this medium. Note that corticosterone in the three solvents present higher solvation energies, as compared with equilenin, equilin and estrone steroids. Besides, in equilenin and estrone steroids are observed volume contractions while in equilin in methanol solution a volume expansion is predicted.

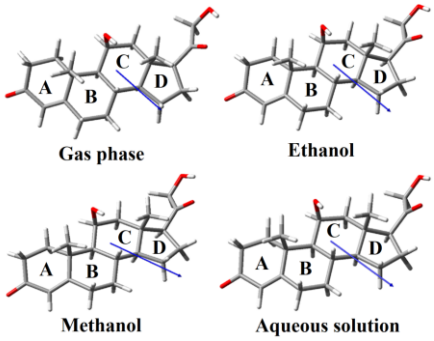

Figure 2. Orientations, magnitudes and directions of dipole moment vectors of corticosterone in different media by using the B3LYP/6-31G* method.

Predicted parameters for corticosterone in gas phase and aqueous, ethanol and methanol solutions by using the B3LYP/6-31G* method are summarized in **Table 3**. The values are compared with the experimental structure determined by X-ray diffraction by Yousuf et al [29] for 21-hydroxypregna-1,4-diene-3,20-dione by using the root-mean-square deviation (RMSD) values. The structural differences between corticosterone and 21-hydroxypregna-1,4-diene-3,20-dione are observed in blue circles in **Figure 3**. Hence, in the compared compound the ring A is nearly planar because presents a C=C bond different from corticosterone and, also, is characterized by the absence of an OH group.

Table 2. Corrected and uncorrected solvation energies (in kJ/mol) by the total non-electrostatic terms for corticosterone in aqueous, ethanol and methanol solutions by using the B3LYP/6-31G* method.

CORTICOSTERONE[a]				
Medium	$\Delta G_{un}^{\#}$	ΔG_{ne}	ΔG_c	ΔV
Aqueous	-75.54	30.56	-106.10	1.5
Ethanol	-98.10	-3.43	-94.67	1.2
Methanol [#]	-100.72	2.88	-103.60	1.1
STEROIDS IN METHANOL[a]				
	$\Delta G_{un}^{\#}$	ΔG_{ne}	ΔG_c	ΔV
Equilenin	-69.51	-1.80	-67.71	-0.4
Equilin	-69.51	-2.88	-66.63	0.6
Estrone	-69.25	-4.05	-65.20	-0.1

ΔG_{un}= uncorrected solvation energy, ΔG_{ne}= total non electrostatic terms, ΔG_c= corrected solvation energies by uncorrected and non-electrostatic solvation energies. [#]Uncorrected by ZPVE; [a]This work

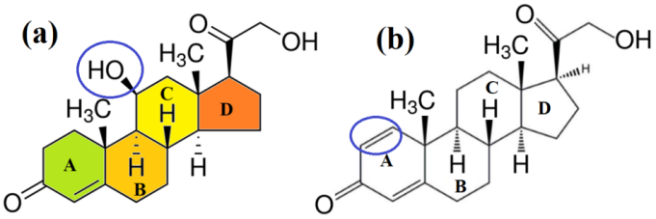

Figure 3. Comparisons between the optimized structure for (a) corticosterone in gas phase by using the hybrid B3LYP/6-31G* level of theory with the experimental one determined for (b) 21-hydroxypregna-1,4-diene-3,20-dione in the solid phase by Yousuf et al [29].

The comparisons in the geometrical parameters of corticosterone in the four media with the corresponding to 21-hydroxypregna-1,4-diene-3,20-dione by using the RMSD values demonstrate: (i) approximately the same values in gas phase and aqueous, ethanol and methanol solutions and, (ii) the better correlations for bond lengths and angles (0.017-0.016 Å and 1.4-1.1 º), as compared with the values predicted for the dihedral angles. Here, very high RMSD values are calculated for the dihedral angles in the four media and, for this reason, the values are not presented in Table 3. The calculations predicted for the dihedral O4-C25-C21-C11, O4-C25-C21-O2 and C17-C6-C5-C13 angles of corticosterone in the four media few differences in the RMSD values but the same signs that the experimental structure of 21-hydroxypregna-1,4-diene-3,20-dione while, on the contrary, the dihedral C25-C21-C11-C6, C20-C9-C16-C18, C20-C9-C16-C23, C17-C6-C5-C7, O2-C21-C11-C6 and O2-C21-C11-C15 angles are predicted in the four media with different signs than those determined for the experimental structure of 21-hydroxypregna-1,4-diene-3,20-dione. Obviously, the differences are attributed to the absence of OH group and to the presence of C=C bond in the compared compound, different from structure of cortiscoteroide.

Table 3. Calculated geometrical parameters of corticosterone in gas phase and aqueous, ethanol and methanol solutions by using the B3LYP/6-31G* method compared with the corresponding experimental values for 21-hydroxypregna-1,4-diene-3,20-dione taken from Ref [29].

Parameters	B3LYP/6-31G* Method[a]				Experimental [b]
	Gas	Aqueous	Ethanol	Methanol	
Bond lengths (Å)					
C12-O1	1.430	1.442	1.439	1.440	
C21=O2	1.222	1.230	1.228	1.229	1.202(3)
C24=O3	1.223	1.239	1.236	1.237	1.231(4)
C25-O4	1.398	1.414	1.411	1.412	1.402(4)
C23=C16	1.349	1.354	1.353	1.354	1.332(4)
C5-C6	1.550	1.550	1.550	1.550	1.542(3)
C7-C8	1.557	1.557	1.557	1.557	1.544(3)
C9-C16	1.532	1.529	1.530	1.530	1.505(4)
C6-C17	1.549	1.545	1.546	1.546	1.525(4)
C9-C20	1.554	1.555	1.554	1.555	1.551(5)
C11-C21	1.514	1.506	1.508	1.507	1.514(4)
C21-C25	1.524	1.517	1.519	1.518	1.500(4)
RMSD	**0.016**	**0.017**	**0.016**	**0.016**	
Bond angles (º)					
C10-C12-O1	111.2	110.8	110.9	110.8	
C8-C12-O1	115.1	114.8	114.9	114.8	
C11-C21-O2	123.2	123.8	123.7	123.7	123.1(3)
C25-C21-O2	118.3	118.0	118.0	118.0	117.8(3)
C21-C25-O4	111.7	111.4	111.4	111.4	112.2(3)
C23-C24-O3	121.8	121.5	121.6	121.5	121.8(3)
C22-C24-O3	122.5	121.7	121.9	121.7	122.2(3)
C11-C6-C17	109.3	109.4	109.4	109.4	109.1(19)
C10-C6-C17	112.3	112.5	112.5	112.5	111.0(2)
C5-C6-C17	112.6	113.0	113.0	113.0	111.8(2)
C8-C9-C20	113.5	114.0	114.0	114.0	111.9(2)
C16-C9-C20	107.4	106.5	106.6	106.5	109.6(2)
C19-C9-C20	109.6	109.9	109.8	109.8	108.0(3)
C11-C21-C25	118.3	118.1	118.1	118.2	119.1(3)
RMSD	**1.1**	**1.4**	**1.4**	**1.4**	
Dihedral angles (º)					
O4-C25-C21-C11	176.1	175.9	176.2	176.2	175.3(3)
O4-C25-C21-O2	-3.9	-4.2	-4.1	-4.1	-5.9(5)
C25-C21-C11-C6	-95.6	-93.7	-94.4	-94.5	80.2(3)
C20-C9-C16-C18	-72.2	-72.8	-73.0	-73.0	65.5(3)
C20-C9-C16-C23	105.4	104.2	104.2	104.0	-118.0(3)
C17-C6-C5-C7	64.6	65.0	65.1	65.1	-60.5(3)
C17-C6-C5-C13	-67.9	-67.6	-67.7	-67.6	-70.7(3)
O2-C21-C11-C6	84.4	86.4	86.0	85.8	-98.5(3)
O2-C21-C11-C15	-35.1	-33.4	-33.9	-34.0	21.1(4)

[a]This work, [b]From Ref [29], Letter Bold: RMSD values

3.2. Atomic charges, Moleculat electrosctatic potentials (MEP) and bond orders (BO).

In corticosterone, the studies related to atomic charges, molecular electrostatic potentials and bond orders are very important parameters taking into account the presence of four fused rings and of acceptors (O atoms of C=O groups) and donors (OH) groups which, are essential factors to predict the good bioavailability when a species is used as a drug, according to

Veber et al. [69]. Hence, in **Table 4** are given the atomic Merz-Kollman (MK) [52] and Mulliken charges, molecular electrostatic potentials and bond orders only calculated for the O atoms of corticosterone in gas phase, aqueous, ethanol and methanol solutions by using the B3LYP/6-31G* method.

Table 4. Atomic Merz-Kollman (MK) and Mulliken charges, molecular electrostatic potentials and bond orders of corticosterone in gas phase and aqueous, ethanol and methanol solutions by using the B3LYP/6-31G* method.

	B3LYP/6-31G* method[a]							
	MK charges[b]				Mulliken charges[b]			
	Gas	Aqueous	Ethanol	Methanol	Gas	Aqueous	Ethanol	Methanol
1 O	-0.700	-0.709	-0.706	-0.708	-0.632	-0.633	-0.632	-0.633
2 O	-0.426	-0.430	-0.430	-0.430	-0.475	-0.480	-0.479	-0.479
3 O	-0.507	-0.508	-0.508	-0.509	-0.483	-0.494	-0.492	-0.493
4 O	-0.619	-0.623	-0.623	-0.624	-0.625	-0.631	-0.630	-0.631
Atoms	MEP[b]				Bond Order			
	Gas	Aqueous	Ethanol	Methanol	Gas	Aqueous	Ethanol	Methanol
1 O	-22.306	-22.305	-22.305	-22.306	1.801	1.798	1.799	1.798
2 O	-22.303	-22.305	-22.305	-22.305	2.036	2.032	2.033	2.032
3 O	-22.346	-22.348	-22.347	-22.348	2.024	2.012	2.014	2.013
4 O	-22.317	-22.321	-22.320	-22.321	1.795	1.786	1.787	1.786

[a]This work, [b]Atomic units (a.u.)

When the atomic MK and Mulliken charges on all O atoms are exhaustively analyzed for corticosterone in the four media the values are practically similar among them but, when their behaviours are graphed in **Figure 4** we can see slight differences between the values of both charges. Thus, in all media the O2 and O3 atoms present the higher values of both charges while the charges on the O1 and O4 atoms have lower values.

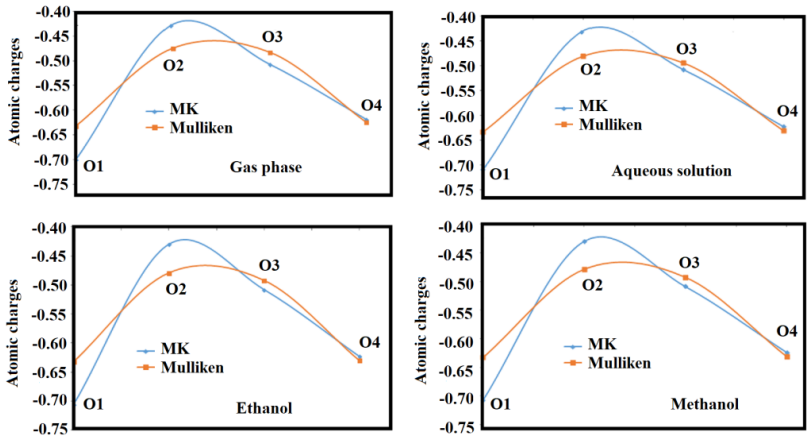

Figure 4. Variations and behaviours of atomic Merz-Kollman (MK) and Mulliken charges on all O atoms of corticosterone in gas phase and aqueous, ethanol and methanol solutions by using the B3LYP/6-31G* method.

These results are the expected because the O2 and O3 belong to two C=O groups while the O1 and O4 atoms belong to two OH groups. Besides, it is observed that the MK charges on the O2 atoms have higher values and lower values are observed on the O1 atoms in the four media while the Mulliken charges on the O3 atoms present the higher values. Note that both charges on the O4 atoms present the same values in the four media. If now, the molecular electrostatic potentials on all O atoms are analyzed from Table 4 the values practically are similar in the four media although notable differences can be seen in the mapped MEP surfaces, as shown in **Figure 5**.

Thus, the O3 atoms present the higher MEP values and, as a consequence strong red colours are observed on these atoms and weak red colours on the O2 and O4 atoms. Here, only the surfaces for corticosterone in gas phase and in aqueous solution are presented because the surfaces for corticosterone in ethanol and methanol are similar to those observed in aqueous solution. In gas phase, it is observed strong blue colours on the H51 and H55 atoms belong to OH groups but the colorations are weak in solution. Evidently, the hydration of these groups in solution justifies the diminishing of colour. On the other hand, green colours typical of inert places are observed on the C=C of ring A while ligth blue colours are also observed on some aliphatic C-H groups.

The red and blue colours are characteristic of nucleophilic and electrophilic sites, respectively where can take place reaction with biological electrophiles and nucleophiles reactive.

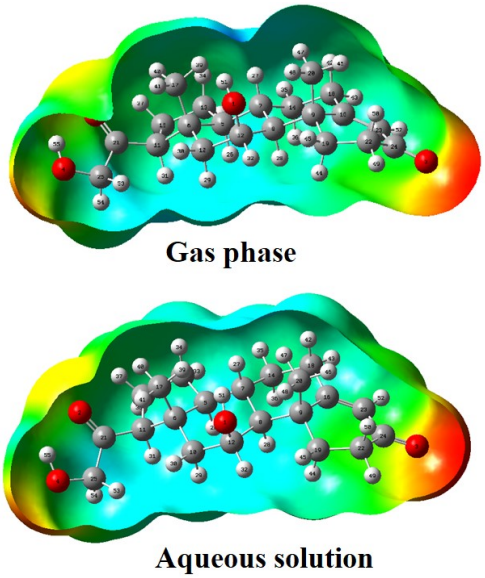

Figure 5. Calculated electrostatic potential surfaces on the molecular surfaces of corticosterone in gas phase and aqueous solution. Color ranges from red to blue are ± 0.058 a.u. B3LYP functional and 6-31G* basis set. Isodensity value of 0.005.

3.3. NBO and AIM studies.

The stabilities studies on equilenin, equilin and estrone steroids have evidenced that equilin is the most stable species, as compared with equilenin and estrone probably due to the presence of an unsaturated C=C bond in the B ring of equilin [9]. These studies are also important in corticosterone taking into account that in the ring A there is a C=C bond. Hence, the main delocalization energies and the topological properties are analyzed for corticosterone in the four media with the NBO and AIM2000 programs by using B3LYP/6-31G* calculations [53,54]. The results can clearly be seen in **Table 5**.

The analyses of main delocalization energies show the presence of three different $\Delta E_{\pi\to\pi^*}$, $\Delta E_{n\to\sigma^*}$ and $\Delta E_{\pi^*\to\pi^*}$ interactions where the higher values are observed for the $\Delta E_{n\to\sigma^*}$ interactions in the four media, as expected because in these interactions are involved the O2 and O3 atoms that belong to the two C=O groups. Hence, the evaluation of the total energies shows a higher stability of corticosterone in gas phase whiles in aqueous solution present the lower value. This latter resulted is in complete agreement with the higher solvation energy observed in this medium because in water corticosterone is most hydrated with solvent molecules than in ethanol and methanol.

The Bader's theory of atoms in molecules (AIM) [70] is of great aid to investigate different types of interactions and, for this reason, for corticosterone in gas phase and aqueous, ethanol and methanol solutions were computed the topological properties with the AIM2000 program [54] in all bond critical points (BCPs) and ring critical points (RCPs) by using the B3LYP/6-31G* method. Hence, the electron density, $\rho(r)$ and the Laplacian values, $\nabla^2\rho(r)$ were calculated in BCPs and RCPs by using the B3LYP/6-31G* method, as in similar species containing rings [1,3-15]. These properties for corticosterone in all media are presented in **Table 6**.

In this work, the other parameters, eigenvalues $(\lambda 1, \lambda 2, \lambda 3)$ of the Hessian matrix and the $|\lambda 1|/\lambda 3$ ratio were no presented in Table 6. Note that in gas phase appear six H bonds interactions which are O1-H48, O2-H40, O2-H55, H27-H39, H39-H51 and H30-H53 interactions while in the three solutions the O2-H40 interactions are no observed probably due to the higher distances between the two involved atoms. This way, the distances in the three solutions are higher than the observed in gas phase of 2.616 Å. Obviously, in the H bonds interactions $\lambda 1/\lambda 3 < 1$ and $\nabla^2\rho(r) > 0$ (closed-shell interaction). New RCPs are observed, as a consequence of H bonds interactions formed, named RCPN1, RCPN2, etc, while the RCPs of the four rings themselves are called A, B, C and D. The formation of six H bonds in gas phase and only five in the solutions indicate that corticosterone is most stable in gas phase than in the three solutions. In **Figure 6** is presented the molecular graphic of corticosterone in gas phase showing all BCPs and RCPs because in this medium present a higher number of new H bonds.

This study clearly suggests the high stability of corticosterone in gas phase and the low stabilities in aqueous, ethanol and methanol solutions due to the new H bonds formed.

3.4. Frontier orbitals and quantum global descriptors studies.

Previous studies by using the gap values on steroids species have revealed that equilenin is the most reactive species than equilin and estrone due probably to its higher global electrophilicity value while higher global nucleophilicty values are observed for equilin and estrone [9]. For corticosterone in gas phase and aqueous, ethanol and methanol solutions were also calculated the gap values by using the frontier orbitals and, with these results were predicted the chemical potential (μ), electronegativity (χ), global hardness (η), global softness (S), global electrophilicity index (ω) and global nucleophilicity index (E) descriptors [59-68]. Hence, in **Table 7** are presented the frontier orbitals, gap and descriptors values for corticosterone in gas phase and aqueous, ethanol and methanol solutions by using the B3LYP/6-31G* method. Note that the equations used to compute all descriptors are also presented in that Table. The results clearly evidence the higher gap value in gas phase and, for this reason, corticosterone is most stable and less reactive in this media while the lower value observed in aqueous solution support the higher reactivity in this medium and the lower stability, as suggested by the NBO studies and by the higher solvation energy. Here, for corticosterone it is observed a higher global electrophilicity value in aqueous solution (2.9814 eV) and a low nucleophilicity index (-9.5229 eV) in this medium, in complete agreement with equilenin steroid [9]. If now the gap values of equilenin (4.5008 eV), equilin (5.4695 eV) and estrone (5.4342 eV) are compared with the observed for corticosterone in the four media equilenin presents the lower value for which its species is the most reactive while corticosterone in all media is most reactive than equilin and estrone. This study shows clearly that the steroid species most reactive, equilenin and corticosterone, are characterized by a high global electrophilicity index value and low nucleophilicity index, having corticosterone a higher electrophilicity index value (2.8068 eV) while equilenin has a lower nucleophilicity index (-7.3851 eV).

Table 5. Main delocalization energies (in kJ/mol) for corticosterone in gas phase and aqueous, ethanol and methanol solutions by using B3LYP/6-31G* calculations.

Delocalization	Gas	Aqueous	Ethanol	Methanol
*πC16-C23→π*O3-C24*	89.91	96.85	95.64	96.43
$\Delta E_{\pi\rightarrow\pi^*}$	89.91	96.85	95.64	96.43
*LP(2)O2→σ*C11-C21*	79.25	77.04	77.62	77.29
*LP(2)O2→σ*C21-C25*	77.79	74.49	75.28	74.95
*LP(2)O3→σ*C22-C24*	88.07	81.43	82.76	82.05
*LP(2)O3→σ*C23-C24*	81.05	74.11	75.45	74.70
$\Delta E_{n\rightarrow\sigma^*}$	326.17	307.06	311.12	308.99
*π*O3-C24→π*C16-C23*	155.29	159.13	160.72	161.01
$\Delta E_{\pi^*\rightarrow\pi^*}$	155.29	159.13	160.72	161.01
ΔE_{Total}	**571.37**	**563.04**	**567.48**	**566.43**

Table 6. Analysis of the Bond Critical Points (BCPs) and Ring critical point (RCPs) for corticosterone in different media by using the B3LYP/6-31G* method.

Parameter[#]	**B3LYP/6-31G* Method[a]**					
	GAS PHASE					
	O1-H48	O2-H40	O2-H55	H27-H39	H39-H51	H30-H53
ρ(r)	0.0163	0.0091	0.0265	0.0101	0.0136	0.0050
$\nabla^2\rho(r)$	0.0561	0.0380	0.0957	0.0396	0.0540	0.0173
Distance, Å	2.304	2.616	2.010	2.136	1.903	2.458
RCPs New						
Parameter[#]	RCPN1	RCPN2	RCPN3	RCPN4	RCPN5	RCPN6
ρ(r)	0.0103	0.0091	0.0243	0.0101	0.0086	0.0045
$\nabla^2\rho(r)$	0.0494	0.0392	0.1428	0.0398	0.0420	0.0169
RCPs Rings						
Parameter[#]	*A*	*B*	*C*	*D*		
ρ(r)	0.0175	0.0170	0.0171	0.0368		
$\nabla^2\rho(r)$	0.1212	0.1062	0.1053	0.2413		
AQUEOUS SOLUTION						
Parameter[#]	O1-H48	O2-H40	O2-H55	H27-H39	H39-H51	H30-H53
ρ(r)	0.0142		0.0274	0.0094	0.0112	0.0056
$\nabla^2\rho(r)$	0.0515		0.0979	0.0372	0.0460	0.0199
Distance, Å	2.379		1.995	2.188	1.976	2.390
RCPs New						
Parameter[#]	RCPN1	RCPN2	RCPN3	RCPN4	RCPN5	RCPN6
ρ(r)	0.0099		0.0247	0.0092	0.0081	0.0048
$\nabla^2\rho(r)$	0.0461		0.1470	0.0408	0.0372	0.0187
RCPs Rings						
Parameter[#]	*A*	*B*	*C*	*D*		
ρ(r)	0.0177	0.0171	0.0172	0.0369		
$\nabla^2\rho(r)$	0.1233	0.1068	0.1064	0.2416		
ETHANOL SOLUTION						
	O1-H48	O2-H40	O2-H55	H27-H39	H39-H51	H30-H53
ρ(r)	0.0147		0.0271	0.0094	0.0112	0.0053
$\nabla^2\rho(r)$	0.0530		0.0972	0.0372	0.0460	0.0186
Distance, Å	2.360		2.000	2.186	1.974	2.425
RCPs New						
Parameter[#]	RCPN1	RCPN2	RCPN3	RCPN4	RCPN5	RCPN6
ρ(r)	0.0101		0.0245	0.0092	0.0080	0.0047
$\nabla^2\rho(r)$	0.0471		0.1457	0.0408	0.0368	0.0179
RCPs Rings						
Parameter[#]	*A*	*B*	*C*	*D*		
ρ(r)	0.0177	0.0170	0.0172	0.0369		
$\nabla^2\rho(r)$	0.1227	0.1064	0.1061	0.2413		
METHANOL SOLUTION						
Parameter[#]	O1-H48	O2-H40	O2-H55	H27-H39	H39-H51	H30-H53
ρ(r)	0.0144		0.0271	0.0094	0.0112	0.0053
$\nabla^2\rho(r)$	0.0522		0.0971	0.0371	0.0458	0.0186
Distance, Å	2.372		2.001	2.187	1.979	2.426
RCPs New						
Parameter[#]	RCPN1	RCPN2	RCPN3	RCPN4	RCPN5	RCPN6

$\rho(r)$	0.0100		0.0245	0.0092	0.0081	0.0047
$\nabla^2\rho(r)$	0.0467		0.1456	0.0408	0.0368	0.0179
RCPs Rings						
Parameter[#]	*A*	*B*	*C*	*D*		
$\rho(r)$	0.0177	0.0170	0.0172	0.0369		
$\nabla^2\rho(r)$	0.1229	0.1064	0.1061	0.2413		

[a]This work, [#]In a.u. units

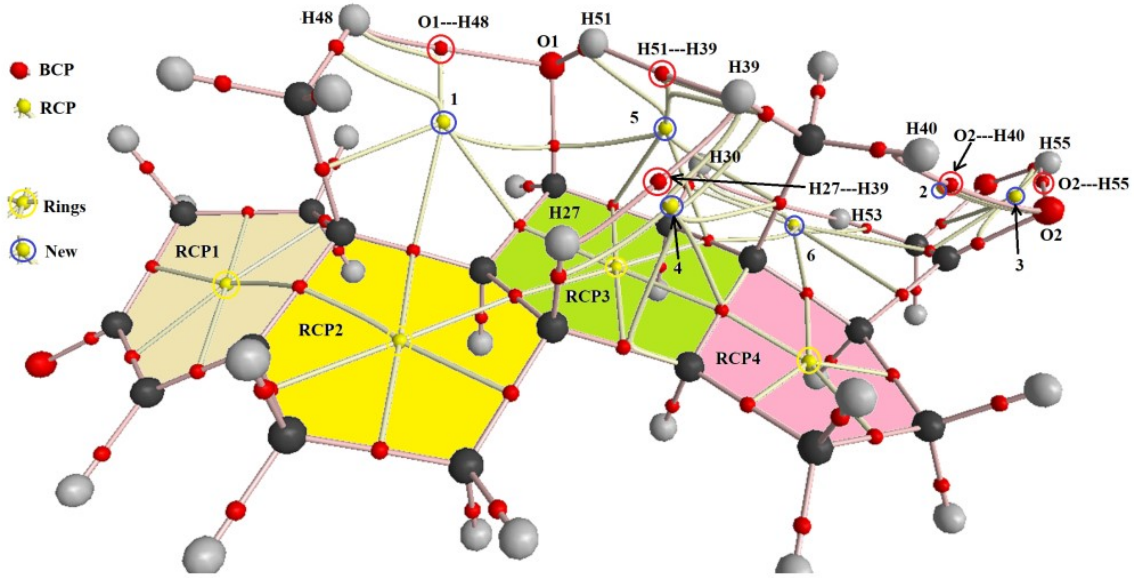

Figure 6. Molecular graphic for corticosterone in gas phase showing the geometries of all its bond critical points (BCPs) and ring critical points (RCPs) by using the B3LYP/6-31G* method.

Table 7. Frontier molecular HOMO and LUMO orbitals, gap values and descriptors (in eV) of corticosterone in gas phase by using the B3LYP/6-31G* method.

B3LYP/6-31G* method[a]				
Orbitals	Gas	Aqueous	Ethanol	Methanol
HOMO	-6.3022	-6.3212	-6.3239	-6.3212
LUMO	-1.2381	-1.3660	-1.3470	-1.3551
GAP	-5.0641	-4.9552	-4.9769	-4.9661
Descriptors				
χ	-2.5321	-2.4776	-2.4885	-2.4831
μ	-3.7702	-3.8436	-3.8355	-3.8382
η	2.5321	2.4776	2.4885	2.4831
S	0.1975	0.2018	0.2009	0.2014
ω	2.8068	2.9814	2.9558	2.9664
E	-9.5462	-9.5229	-9.5443	-9.5303

[a]This work

χ = - [E(LUMO)- E(HOMO)]/2 ; μ = [E(LUMO) + E(HOMO)]/2; η = [E(LUMO) - E(HOMO)]/2; $S = \frac{1}{2}\eta$; $\omega = \mu^2/2\eta$; $E=\mu*\eta$

A very important resulted derived from this study is that both global electrophilicity and nucleophilicity indexes are independent of number of C=O and OH groups because in the steroids species only a C=O group and one OH group are observed while in corticosterone two groups of each one are present in its structure. Evidently, other different properties are related to those two predictors.

3.5. Vibrational study.

The optimized structures of corticosterone in all media were predicted with C_1 symmetries by using the hybrid B3LYP/6-31G* level of theory while the expected numbers of vibration modes are 159 and where all them show activity in both spectra.

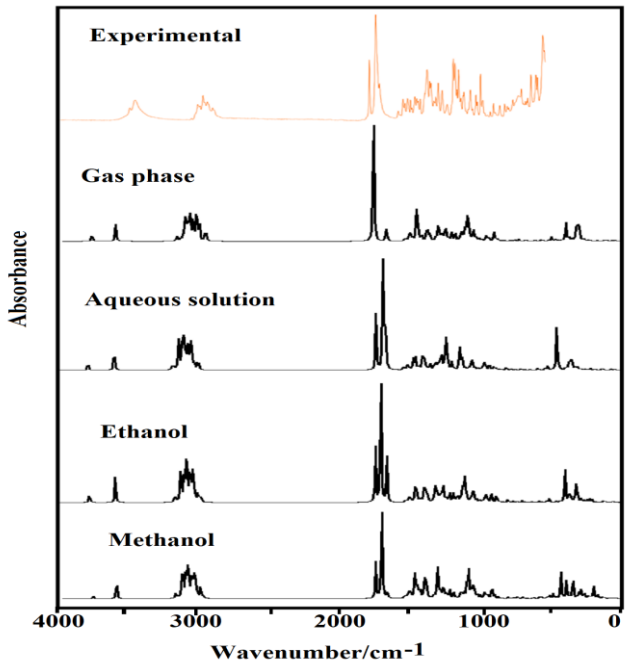

Figure 7. Experimental available IR spectrum of cortiscoterone in solid phase [56] compared with the predicted in gas phase and aqueous, ethanol and methanol solutions by using the hybrid B3LYP/6-31G* method.

The experimental available infrared and Raman spectra were taken from the literature [56] and are given in **Figures 7** and **8** compared with the corresponding predicted in gas phase and aqueous, ethanol and methanol solutions by using the same level of theory. Here, only the bands observed in the attenuated total reflectance (ATR) were considered because the intensities of bands observed in the IR spectrum in the higher wavenumber region are similar to the corresponding predicted while the bands

observed in the ATR spectrum present higher intensities than the theoretical ones, as shown in **Figure 9**.

On the other hand, the complete assignments were performed by using the SQMFF procedure and the Molvib program, as indicated in section Mechanical quantum calculations [16-18]. The observed and calculated wavenumbers and assignments for cortiscoterone in the gas phase and ethanol and methanol solutions are presented in **Table 8**. Later, brief discussions on assignments of some groups are discussed below.

3.6. Band Assignments.

4000-2000 cm^{-1} region. This region is characteristic of stretching modes of C-H, OH, CH_3 and CH_2 groups. Hence, the SQM calculations predicted the two OH stretching modes of cortiscoterone in all media between 3624 and 3443 cm^{-1}, as expected, for which the IR and ATR bands located between 3465 and 3412 cm^{-1} are easily assigned to these vibration modes. Obviously, the only aromatic C23-H53 stretching modes in all media are predicted by calculations at higher wavenumbers than the other ones, hence, the weak Raman band at 3053 cm^{-1} is assigned to those stretching modes. The aliphatic C-H stretching modes of cortiscoterone in the different media are predicted in different regions and, for these reasons, these modes are assigned accordingly. In the same way, the SQM/B3LYP/6-31G* calculations have predicted the antisymmetric and symmetric stretching modes of CH_3 and CH_2 groups of cortiscoterone in all media in different regions and, therefore, the IR and Raman bands between 3036 and 2934 cm^{-1} are assigned to stretching modes of CH_3 groups while the stretching modes of CH_2 groups are associated to bands between 3004 and 2844 cm^{-1}. The symmetries of those stretching modes can be seen in detailed form in Table 8 where the bands of media intensities are assigned to symmetrical modes.

2000-1000 cm^{-1} region. In corticosterone are expected two C=O stretching modes, one C=C stretching mode, two C-O stretching modes and, moreover, other C-C stretching modes. In this region are also assigned the OH deformation modes, deformation, wagging and rocking modes of CH_2 groups, deformation and rocking modes of CH_3 groups and C-H rocking modes [1-9,60-64]. Some of these vibration modes in gas phase and ethanol and methanol solutions are predicted in different regions while other modes, as C=O and C=C stretching modes, are predicted at higher wavenumbers and in the same regions in the three media. Hence, the most intense IR, ATR and Raman bands between 1705 and 1602 cm^{-1} are clearly assigned to C=O and C=C stretching modes, as in similar species [7,9,10,12,14,60,63,64]. The two OH deformation modes are predicted in the same regions and, hence, they are assigned to the shoulder and IR band at 1268 and 1224 cm^{-1}. The antisymmetric deformations of CH_3 groups are assigned to the bands between 1488 and 1466 cm^{-1} while the corresponding symmetric modes are associated with the bands between 1394 and 1357 cm^{-1}. The CH_3 rocking modes are assigned between 1120 and 922 cm^{-1}. The deformation, wagging, rocking and twisting modes of CH_2 groups are respectively assigned to the bands 1458/1413, 1429/1277, 1345/1160 and 990/654 cm^{-1}. The C5-C6, C5-C13, C7-C8, C10-C12 and C19-C22 stretching modes are predicted in the same regions in the three media and, for these reasons, they are assigned accordingly.

1000-10 cm^{-1} region. In this region, for cortiscoterone in the different media are expected C-C stretching modes, C-H out-of-plane deformation, CH_2 and CH_3 twisting modes, deformations and torsions of four rings and torsions of OH groups. The assignments of all those modes are clearly detailed in Table 8 where it is observed a strong coupling of some vibration modes in the lower wavenumbers region, such as different torsion modes of OH and CH_3 groups and of rings. Other skeletal modes as, CCO and CCC deformation modes and rocking of C-CH_3 groups are also predicted in this region. Here, only the vibration modes predicted by SQM calculations until 156 cm^{-1} have been assigned because the Raman spectrum was recorded from 3500 up to 160 cm^{-1}.

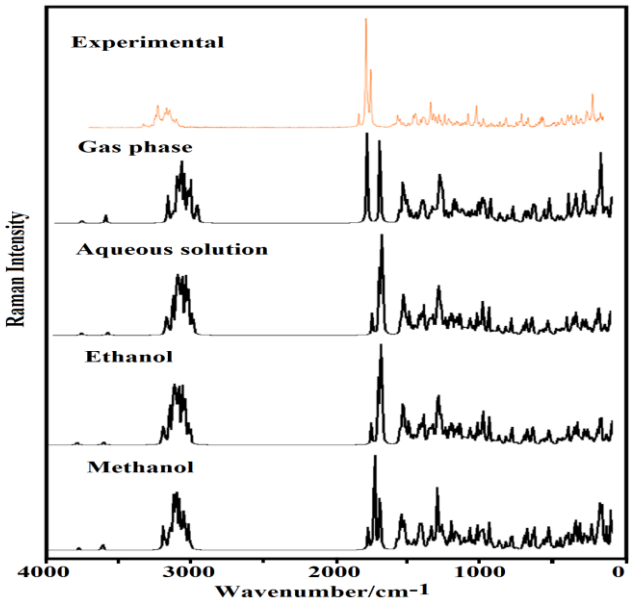

Figure 8. Experimental available Raman spectrum of cortiscoterone in solid phase [56] compared with the predicted in gas phase and aqueous, ethanol and methanol solutions by using the hybrid B3LYP/6-31G* method.

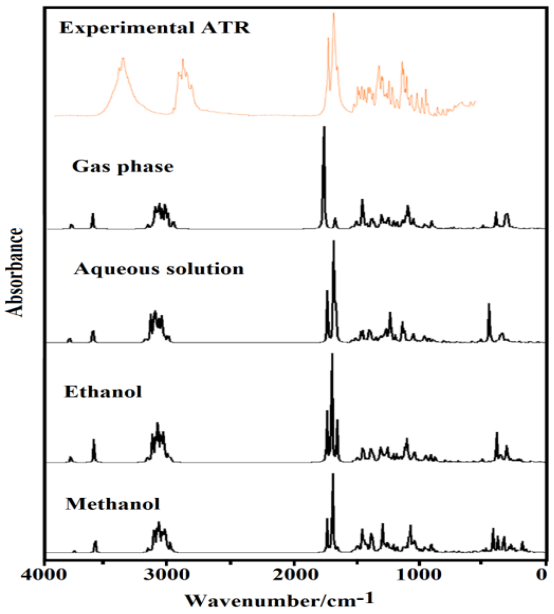

Figure 9. Experimental available ATR spectrum of cortiscoterone in solid phase [56] compared with the predicted in gas phase and aqueous, ethanol and methanol solutions by using the hybrid B3LYP/6-31G* method.

Table 8. Observed and calculated wavenumbers (cm^{-1}) and assignments of cortiscoterone in gas phase and ethanol and methanol solutions by using the B3LYP/6-31G* method.

Experimental			B3LYP/6-31G* Method[a]					
			Gas		Ethanol		Methanol	
IR[c]	ATR[c]	Raman[e]	SQM[b]	Assignments[a]	SQM[b]	Assignments[a]	SQM[b]	Assignments[a]
3465w	3443s		3624	νO1-H51	3617	νO1-H51	3603	νO1-H51
3422w	3412s		3465	νO4-H55	3443	νO4-H55	3446	νO4-H55
		3053w	3047	νC23-H52	3040	νC23-H52	3044	νC23-H52
3036vw		3037w	3042	ν_aCH_3(C20)	3032	ν_aCH_3(C20)	3031	ν_aCH_3(C20)
			3018	ν_aCH_3(C17)	3004	ν_aCH_3(C17)	3008	ν_aCH_3(C17)
3000vw		3004w	3004	ν_aCH_2(C15)	2997	ν_aCH_2(C15)	3000	ν_aCH_2(C15)
			2990	ν_aCH_3(C20)	2996	ν_aCH_3(C20)	2996	ν_aCH_3(C17)
			2989	ν_aCH_3(C17)	2995	ν_aCH_3(C17)	2992	ν_aCH_3(C20)
	2986w	2983sh	2982	ν_aCH_2(C22)	2976	ν_aCH_2(C13)	2977	ν_aCH_2(C13)
2976sh		2976sh	2980	ν_aCH_2(C13)	2974	ν_aCH_2(C22)	2976	ν_aCH_2(C22)
			2972	νC12-H32	2972	ν_aCH_2(C19)	2972	ν_aCH_2(C19)
		2965m	2966	ν_aCH_2(C19)	2962	ν_aCH_2(C18)	2964	νC12-H32
		2965m	2962	ν_aCH_2(C18)	2961	νC12-H32	2963	ν_aCH_2(C18)
2956w		2957sh	2956	ν_aCH_2(C14)	2957	ν_aCH_2(C14)	2959	ν_aCH_2(C14)
			2954	ν_sCH_2(C15)	2954	ν_sCH_2(C15)	2954	ν_aCH_2(C10)
	2945m		2953	ν_aCH_2(C10)	2952	ν_aCH_2(C10)	2953	ν_sCH_2(C15)
2938w	2936sh	2938w	2938	ν_sCH_3(C20)	2939	ν_sCH_3(C17)	2939	ν_sCH_3(C17)
			2934	ν_sCH_3(C17)	2939	ν_sCH_3(C20)	2937	ν_sCH_3(C20)
			2931	ν_sCH_2(C13)	2936	νC11-H31	2931	ν_sCH_2(C13)
2916m	2921sh	2919w	2915	ν_sCH_2(C22)	2930	ν_sCH_2(C13)	2929	νC11-H31
			2914	νC11-H31	2929	ν_aCH_2(C25)	2918	ν_sCH_2(C19)
2906sh	2906s	2909m	2907	ν_sCH_2(C14)	2919	ν_sCH_2(C19)	2918	ν_aCH_2(C25)
			2905	ν_sCH_2(C19)	2914	νC7-H27	2911	νC7-H27
	2895sh		2902	ν_sCH_2(C10)	2910	ν_sCH_2(C10)	2907	ν_sCH_2(C10)
		2890m	2897	νC7-H27	2910	ν_sCH_2(C22)	2906	ν_sCH_2(C22)
2884sh		2890m	2893	ν_sCH_2(C18)	2903	ν_sCH_2(C18) ν_sCH_2(C14)	2901	ν_sCH_2(C14)
2877sh	2875m	2890m	2890	ν_aCH_2(C25)	2898	ν_sCH_2(C18) ν_sCH_2(C14)	2895	ν_sCH_2(C18)
		2866sh	2857	νC8-H28	2883	ν_sCH_2(C25)	2875	ν_sCH_2(C25)
2844w		2849w	2849	ν_sCH_2(C25)	2872	νC8-H28	2871	νC8-H28
2834sh	2833m	2842sh	2847	νC5-H26	2857	νC5-H26	2856	νC5-H26
1680s	1676s	1705w	1716	νC21=O2	1680	νC21=O2	1685	νC21=O2
1632vs	1633vs	1657vs	1710	νC24=O3	1643	νC24=O3	1645	νC24=O3
1602s	1602m	1626s	1624	νC16-C23	1603	νC16-C23	1608	νC16-C23
1511sh		1488vw	1490	δ_aCH_3(C17), δ'_aCH_3(C17)	1468	δ'_aCH_3(C17) δ_aCH_3(C17)	1486	δ_aCH_3(C20)
			1485	δ_aCH_3(C20)	1460	δ_aCH_3(C20)	1479	δCH_2(C13)
			1478	δCH_2(C13) δCH_2(C15)	1456	δCH_2(C13)	1474	δ_aCH_3(C17)
1466w	1460w	1466sh	1465	δ_aCH_3(C20)	1449	δ_aCH_3(C20)	1467	δ_aCH_3(C20)
1466w	1460w	1466sh	1462	δ'_aCH_3(C17) ,δ_aCH_3(C17)	1449	δ_aCH_3(C17) δ'_aCH_3(C17)	1459	δ_aCH_3(C17)
		1458m	1458	δCH_2(C19)	1446	δCH_2(C25) $wagCH_2$(C25)	1457	δCH_2(C19)
			1457	δCH_2(C14)	1443	δCH_2(C19)	1456	δCH_2(C14)
			1455	δCH_2(C13) δCH_2(C15)	1442	δCH_2(C14)	1454	δCH_2(C13) δCH_2(C15)

Experimental			B3LYP/6-31G* Method[a]					
			Gas		Ethanol		Methanol	
IR[c]	ATR[c]	Raman[e]	SQM[b]	Assignments[a]	SQM[b]	Assignments[a]	SQM[b]	Assignments[a]
1446sh			1455	δCH_2(C25)	1440	δCH_2(C15)	1446	δCH_2(C25)
		1442w	1443	δCH_2(C18)	1430	δCH_2(C10)	1441	δCH_2(C18)
	1432m	1442w	1442	δCH_2(C10)	1425	δCH_2(C18)	1440	δCH_2(C10)
1429m		1423w	1427	δCH_2(C22)	1410	δCH_2(C25) $wagCH_2$(C25)	1427	δCH_2(C22)
1413m	1416m	1416sh	1415	ρC12-H32	1409	δCH_2(C22)	1415	$wagCH_2$(C25) δCH_2(C25)
		1416sh	1415	$wagCH_2$(C25)	1408	ρC12-H32	1403	ρC12-H32
1398sh	1394m	1399sh	1402	ρ'C5-H26	1397	ρ'C5-H26	1401	ρ'C5-H26
1394m		1390w	1393	$\delta_s CH_3$(C17)	1387	$wagCH_2$(C10)	1393	$\delta_s CH_3$(C17)
1387sh			1386	$wagCH_2$(C19)	1383	$wagCH_2$(C19)	1386	$wagCH_2$(C19)
			1379	ρ'C12-H326	1377	ρ'C12-H326	1381	ρ'C12-H326 $wagCH_2$(C10)
1372m	1375m		1373	$wagCH_2$(C14)	1372	$wagCH_2$(C14)	1375	$wagCH_2$(C14)
		1368sh	1371	$\delta_s CH_3$(C20) ρC8-H28	1365	ρC8-H28	1370	$\delta_s CH_3$(C20) ρC8-H28
1363w	1363sh	1357m	1363	$wagCH_2$(C19)	1362	ρC11-H31	1364	$\delta_s CH_3$(C20)
		1357m	1360	ρC11-H31 $wagCH_2$(C10)	1360	$\delta_s CH_3$(C20)	1362	ρC11-H31
		1357m	1356	$wagCH_2$(C18)	1350	$wagCH_2$(C18)	1357	$wagCH_2$(C18)
1342m	1342m	1345m	1348	ρC5-H26	1345	$wagCH_2$(C22) ρCH_2(C19)	1351	ρCH_2(C19)
1342m	1342m	1345m	1347	$wagCH_2$(C22) ρCH_2(C19)	1343	ρC5-H26	1348	ρC5-H26
		1337sh	1336	βC23-H52 νC9-C16	1336	ρCH_2(C14) $wagCH_2$(C18)	1343	νC9-C16
1327m	1327m		1326	ρ'C8-H28	1324	ρ'C8-H28	1325	ρ'C8-H28
1318m	1320sh	1315sh	1321	$wagCH_2$(C13)	1318	$wagCH_2$(C15) $wagCH_2$(C13)	1321	$wagCH_2$(C15) $wagCH_2$(C13)
		1311w	1304	$wagCH_2$(C15)	1301	$wagCH_2$(C15)	1304	$wagCH_2$(C15)
	1300w	1301sh	1301	ρ'C7-H27	1296	ρ'C7-H27	1300	ρ'C7-H27
1298m		1297m	1297	$wagCH_2$(C13) ρ'C12-H326	1292	$wagCH_2$(C13) $wagCH_2$(C15)	1296	$wagCH_2$(C13) ρ'C12-H326
		1288sh	1283	ρ'C12-H326	1279	$wagCH_2$(C22)	1285	$wagCH_2$(C22)
		1277sh	1273	$wagCH_2$(C22)	1272	ρ'C11-H31	1278	ρ'C12-H326
1268sh	1270sh		1271	δO4-H55	1264	δO4-H55	1264	δO4-H55 $wagCH_2$(C25)
		1260sh	1259	ρC7-H27	1257	ρC7-H27	1259	ρC7-H27
1250s	1250s	1250s	1256	ρCH_2(C10) ρ'C11-H31	1251	ρCH_2(C10) ρ'C11-H31	1255	ρCH_2(C10)
1231s	1228s	1232m	1232	νC23-C24	1234	βC23-H52	1238	βC23-H52
1224s			1227	δO1-H51	1229	δO1-H51	1227	ρCH_2(C14) δO1-H51
1224s			1224	ρCH_2(C15)	1224	ρCH_2(C25)	1224	ρCH_2(C15) ρCH_2(C13)
	1217s	1214m	1216	ρCH_2(C18)	1216	ρCH_2(C15) ρCH_2(C13)	1212	ρCH_2(C18) ρCH_2(C13)
			1208	ρCH_2(C13)	1209	ρCH_2(C18)	1207	ρCH_2(C19)
1200m	1200w	1198m	1206	ρCH_2(C25)	1205	νC6-C10	1198	ρCH_2(C25)

Experimental			B3LYP/6-31G* Method[a]					
			Gas		Ethanol		Methanol	
IR[c]	ATR[c]	Raman[e]	SQM[b]	Assignments[a]	SQM[b]	Assignments[a]	SQM[b]	Assignments[a]
1186m	1186w	1188w	1185	ρCH_2(C22)	1182	ρC7-H27	1188	ρCH_2(C22)
1167s	1167m		1179	νC9-C19	1181	ρCH_2(C22)	1182	ρC7-H27
1160sh		1161m	1162	ρCH_2(C18)	1157	ρCH_2(C14)	1156	ρCH_2(C14) δO1-H51,ρCH_2(C18)
1141s	1138m	1137m	1153	νC5-C6	1148	νC5-C6	1154	νC5-C6
1135sh		1130sh	1135	νC5-C7	1136	νC5-C7	1137	νC18-C16
		1120sh	1122	$\rho'CH_3$(C20) ρCH_3(C20)	1125	νC25-O4	1121	$\rho'CH_3$(C20) νC8-C9
		1115sh	1118	νC25-O4 βC21=O2	1118	$\rho'CH_3$(C20) νC8-C9	1112	βC21=O2 νC11-C21
1102m	1099w	1100w	1107	$\rho'CH_3$(C17)	1107	$\rho'CH_3$(C17)	1106	$\rho'CH_3$(C17)
1095sh		1086m	1099	νC5-C13	1099	νC5-C13	1100	νC5-C13
		1086m	1090	νC5-C7 νC18-C16	1090	νC5-C7	1088	νC5-C7 νC5-C13
		1077w	1075	τR_1(A3)	1071	νC25-O4	1072	τR_1(A3)
1054s	1054s	1058w	1065	νC25-O4 νC11-C21	1066	νC11-C21	1054	νC7-C14
	1045s	1047w	1049	νC7-C14	1050	νC7-C14	1046	νC25-O4
1043s		1033w	1043	νC7-C8	1042	νC7-C8	1042	νC7-C8
1028m	1025w	1020sh	1025	νC12-O1 νC10-C12	1016	νC12-O1 νC10-C12	1018	νC10-C12
1016s	1018m	1015m	1015	νC14-C18	1014	νC9-C19	1016	νC9-C19
	1000w	1004sh	1000	νC19-C22	1001	νC19-C22	1002	νC19-C22
999m		991vw	997	νC5-C6	997	$\rho'CH_3$(C17)	998	νC19-C22
			990	$\tau_w CH_2$(C13)	986	$\tau_w CH_2$(C13)	989	$\tau_w CH_2$(C13)
983sh	979sh	975sh	984	νC15-C11	983	νC15-C11	982	νC15-C11
977m	975w	968sh	969	νC13-C15	966	νC13-C15 νC14-C18	969	νC13-C15 νC14-C18
		961s	952	νC13-C15	949	νC13-C15	952	νC13-C15
942w		944w	940	βR_1(A2)	936	βR_1(A2)	939	νC13-C15
	931m		938	γC23-H52 ρCH_3(C20)	931	ρCH_3(C20)	938	γC23-H52
929m	922sh	923sh	929	νC6-C10	925	ρCH_3(C20) νC9-C16	929	ρCH_3(C20) νC6-C10
916w		919m	915	γC23-H52	911	$\tau_w CH_2$(C25) νC6-C11 ρCH_3(C17)	916	γC23-H52 βR_1(A2)
892sh	913sh	912sh	912	$\tau_w CH_2$(C25) νC6-C11 ρCH_3(C17)	908	γC23-H52	911	$\tau_w CH_2$(C25) νC6-C11 ρCH_3(C17)
886m	887w	888w	886	νC13-C15	886	νC15-C11 νC21-C25	887	νC21-C25
	879sh		881	νC21-C25	882	νC15-C11	884	γC23-H52
		870w	880	νC15-C11	876	$\tau_w CH_2$(C18)	883	γC23-H52
853s	855m	854w	858	νC9-C20	854	γC23-H52 νC9-C20	860	$\tau_w CH_2$(C18) νC9-C20
836m	835w	833w	831	$\tau_w CH_2$(C10)	832	νC24-C22 νC23-C24	833	νC24-C22 νC23-C24

Experimental			B3LYP/6-31G* Method[a]					
			Gas		Ethanol		Methanol	
IR[c]	ATR[c]	Raman[e]	SQM[b]	Assignments[a]	SQM[b]	Assignments[a]	SQM[b]	Assignments[a]
824w	829sh	814w	822	$\tau_w CH_2$(C10)	820	$\tau_w CH_2$(C10)	822	$\tau_w CH_2$(C10) νC12-O1
803w	802w	807w	810	νC6-C11	809	νC6-C11	810	νC6-C11
781w	782w	793	785	νC6-C17	783	$\tau_w CH_2$(C15) νC6-C17	786	$\tau_w CH_2$(C15) νC6-C17,$\tau_w CH_2$(C13)
757m	757w	775m	757	$\tau_w CH_2$(C14) νC8-C12	756	$\tau_w CH_2$(C14) νC8-C12	758	$\tau_w CH_2$(C14) νC8-C12
746w	741w	746w	749	βR_1(A3)	750	βR_1(A3)	752	βR_1(A3)
		741sh	743	βC21=O2	743	δC21C25O4 βC21=O2	745	δC21C25O4
		741sh	737	$\tau_w CH_2$(C19) νC24-C22	738	$\tau_w CH_2$(C19)	739	$\tau_w CH_2$(C19)
709m	708w	711w	722	βR_2(A4)	720	βR_2(A4)	720	βR_2(A4)
674m	673w	691w	674	τR_2(A1) ButtC16-C9	678	τR_2(A1)	676	ButtC16-C9
654w	656w	679m	662	$\tau_w CH_2$(C15) δC6C11C21	659	δC6C11C21	661	δC6C11C21
643w	645w	650w	650	γC24=O3	651	γC24=O3	653	γC24=O3
612w	612w	637m	621	βR_1(A4)	622	βR_1(A4)	622	βR_1(A4)
590sh		587w	610	δC8C12O1,βR_2(A3)	612	δC8C12O1	608	δC8C12O1,βR_2(A3)
571m	561sh	572w	563	γC21=O2	566	γC21=O2	563	γC21=O2
551s		559m	551	βR_2(A4)	552	βR_2(A4)	552	βR_2(A4)
521w	547w	549m	522	$\tau_w CH_2$(C22) βR_1(A1)	526	$\tau_w CH_2$(C22) γC24=O3,βR_1(A1)	530	$\tau_w CH_2$(C22) βR_1(A1)
	542w	542m	521	βR_2(A2)	520	βC24=O3,βR_2(A2) δC10C12O1	521	βC24=O3
510w		518w	518	βC24=O3	519	βR_2(A1)	520	βR_2(A2)
503w	501w	490sh	501	βR_3(A1) βR_3(A2)	501	βR_3(A2) δC10C12O1	503	δC10C12O1
479s	477w	481w	466	γC21=O2 ρC6-C17	464	γC21=O2 ρC6-C17	468	γC21=O2 ρC6-C17
		470w	450	βR_3(A1),βR_2(A1)	451	βR_3(A1),βR_2(A1)	452	βR_3(A1),βR_2(A1)
439s	444sh	450w	422	βR_3(A2)	422	βR_3(A2)	422	βR_3(A2),βR_3(A3)
431s		428w	407	βR_3(A1)	407	βR_3(A3)	407	βR_3(A1)
391vs		386m	387	ρ'C6-C17	384	ρ'C6-C17	396	τO4-H55
379sh		374sh	381	ρC9-C20	380	ρC9-C20	383	ρ'C6-C17
		363m	369	τO4-H55	365	ρ'C9-C20,βR_2(A2)	382	ρC9-C20
		363m	364	τO4-H55 ρC6-C17	357	δC21C25O4 βC21=O2	364	ρ'C9-C20
		359sh	354	δC21C25O4	340	τO1-H51	358	δC21C25O4
		332m	335	δC15C11C21 δC10C12O1	338	δC15C11C21	337	δC15C11C21
		312sh	312	τR_1(A2)	309	βR_2(A3)	322	τO1-H51
		303w	307	ButtC16-C9	295	τR_2(A2),τR_1(A2) ButtC16-C9	308	δC10C12O1 ρ'C6-C17
		296sh	295	τO1-H51,τR_2(A2)	294	τO4-H55	293	τR_1(A2)
		278sh	283	τO1-H51,τR_2(A2)	277	τR_2(A1),τR_2(A2)	275	τR_2(A1),τO1-H51
		269m	272	ρ'C9-C20	267	ButtC5-C6	263	ButtC5-C6
		259sh	259	ButtC5-C6	252	$\tau_w CH_2$(C17)	256	ρ'C9-C20

Experimental			B3LYP/6-31G* Method[a]					
			Gas		Ethanol		Methanol	
IR[c]	ATR[c]	Raman[e]	SQM[b]	Assignments[a]	SQM[b]	Assignments[a]	SQM[b]	Assignments[a]
		253sh	252	$\tau_w CH_3$(C20)	251	$\tau_w CH_3$(C20) ρ'C9-C20	251	$\tau_w CH_3$(C20)
		240sh	236	δC11C21C25	234	δC11C21C25	230	δC11C21C25
		233vs	226	τR_2(A1) ButtC7-C8	227	ButtC7-C8	226	τR_2(A1)
		224sh	217	$\tau_w CH_3$(C17),τR_1(A3)	214	$\tau_w CH_3$(C17)	214	τR_1(A1)
		198sh	206	τR_1(A1)	202	τR_1(A1)	201	$\tau_w CH_3$(C20)
		186sh	194	$\tau_w CH_3$(C20) τR_1(A1)	199	$\tau_w CH_3$(C20) τR_1(A1)	186	$\tau_w CH_3$(C17) τO1-H51
		183m	174	τR_2(A4)	174	τR_2(A4)	178	τR_2(A4)
		178sh	166	τR_3(A2)	167	τR_3(A2),τR_1(A3)	163	τR_2(A1),τR_3(A2)
		167w	156	τR_1(A1), τR_2(A1)	159	τR_1(A1)	159	ButtC7-C8
			131	τR_2(A3)	128	τR_2(A3)	130	τR_2(A3),τR_2(A2)
			119	τC25-C21,τO4-H55	118	τC25-C21	122	τC25-C21
			108	τC25-C21,τR_1(A4)	107	τR_1(A4)	112	τR_1(A4),τR_3(A3)
			76	τC25-C21,τR_2(A2)	80	τC21-C11	87	τR_2(A2), τR_2(A4)
			60	τR_3(A1)	60	τR_3(A1)	70	τR_3(A1),τR_3(A2)
			51	τC25-C21 τO4-H55	53	τR_3(A1) τC25-C21	56	τR_2(A2)
			39	τC21-C11	44	τR_2(A2),τR_2(A3)	40	τC21-C11
			28	τR_3(A3)	28	τR_3(A3)	32	τR_3(A3),τC21-C11

Abbreviations: ν, stretching; δ, deformation in the plane; γ, deformation out of plane; wag, wagging; τ, torsion; β_R, deformation ring τ_R, torsion ring; ρ, rocking; τw, twisting; δ, deformation; a, antisymmetric; s, symmetric; (A_1), Ring A; (A_2), Ring B; (A_3), Ring C; (A_4), Ring D. [a]This work, [b]From scaled quantum mechanics force field, [c]From Ref [56].

3.7. Force Fields.

Here, the harmonic force constants for cortiscoterone in gas phase and aqueous, ethanol and methanol solutions were calculated from its corresponding force fields by using the B3LYP/6-31G* method and, later the results were compared in **Table 9** with those reported for equilenin, equilin and estrone steroids [9]. First, when the force constants values for corticosterone in different media are analyzed it is observed that some constants values in gas phase are different from those computed in the three solutions, evidencing this way, higher differences in the *f(νC=O), f(νO-H), f(νC-O), f(νC-CH₃), f(δCH₂)* and *f(δOH)* force constants in aqueous solution. Such variations are attributed to the higher hydration of the involved groups by water molecules due to the higher solvation energy predicted for cortiscoterone in this medium. If now the values for corticosterone are compared with the values for equilenin, equilin and estrone steroids, in general, it is observed higher values in the force constants of these steroids, with exception of *f(νCH₂)* and $f(\nu C\text{-}H)_{A,B}$ force constants that practically present similar values. These differences in the values could be associated with the presence of two C=O and OH groups in the structure of cortiscoterone while in those steroids only one C=O group and one OH group can be observed.

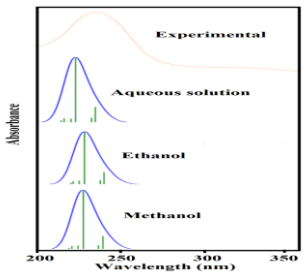

Figure 9. Experimental ultraviolet spectrum of corticosterone in methanol solution compared with the corresponding predicted in aqueous, ethanol and methanol solutions by using B3LYP/6-31G* level of theory.

3.8. Electronic spectra.

The ultraviolet spectra of corticosterone in aqueous, ethanol and methanol solutions were predicted by using the time-dependent DFT calculations (TD-DFT) with the B3LYP/6-31G* method [18]. These spectra are compared in **Figure 9** with the experimental available taken from Ref [56]. In the experimental spectrum are observed a strong band at 235 nm and a should at 315 nm while in the three theoretical spectra only intense bands at c.a. 222.15, 221.85 and 222.05 nm are predicted respectively in aqueous, ethanol and methanol solutions. Clearly, the most intense band could be attributed to the π→π* transitions due to the presence of C=C double bonds while the most weak band could be associated to n→σ * transitions of C=O groups, as were predicted by NBO studies.

4. CONCLUSIONS

In the present work, structural, electronic, topological and vibrational properties of corticosterone hormone have been investigated in aqueous, ethanol and methanol solutions by using DFT calculations and experimental available infrared, attenuated total reflectance (ATR), Raman and Ultraviolet spectra.

The structures of corticosterone were determined theoretically in gas phase and the different solvents at the B3LYP/6-31G* level of theory. All predicted properties in the three solutions were compared with the values obtained in gas phase.

The universal solvation model has evidenced higher solvation energy for corticosterone in aqueous solution and a higher value in methanol, as compared with the corresponding values to equilenin, equilin and estrone steroids in the same medium.

The MK charges on the O atoms are different from the Mulliken ones. Higher Mulliken charges on O atoms of C=O group of side chain are observed in the three solvents than the corresponding to C=O group of ring A while the MK charges on O atoms of OH group of ring C present higher values than the corresponding to O atoms of OH group of side chain.

The natural bond orbital (NBO) studies have revealed a low stability of corticosterone in aqueous solution, as compared with the values in ethanol and methanol solutions, in total agreement with the higher solvation energy and dipole moment values in this medium. On the other hand, the atoms in molecules (AIM) analyses support the lower stabilities of corticosterone in the three solutions.

The gap values suggest that corticosterone is most reactive in aqueous solution than the other solutions, as supported by the low stability and higher solvation energy and dipole moment values in this medium. This study shows clearly that the steroid species most reactive, equilenin and corticosterone, are characterized by a high global electrophilicity index value and low nucleophilicity index.

Reasonable correlations in the predicted IR, Raman and UV spectra were found, as compared with the corresponding experimental ones.

Additionally, the complete vibrational assignments of all 159-vibration modes of corticosterone together with the harmonic force fields and force constants in the different media are for the first time presented.

5. REFERENCES

1. Brandán, S.A. Why morphine is a molecule chemically powerful. Their comparison with cocaine. *Indian Journal of Applied Research* **2017**, *7*, 511-528.
2. Rudyk, R.A.; Brandán, S.A. Force field, internal coordinates and vibrational study of alkaloid tropane hydrochloride by using their infrared spectrum and DFT calculations. *Paripex A Indian Journal of Research* **2017**, *6*, 616-623.
3. Romani, D.; Brandán, S.A. Vibrational analyses of alkaloid cocaine as free base, cationic and hydrochloride species based on their internal coordinates and force fields. *Paripex A Indian Journal of Research* **2017**, *6*, 587-602.
4. Iramain, M.A.; Ledesma, A.E.; Brandán, S.A. Analyzing the effects of halogen on properties of a halogenated series of R and S enantiomers analogues alkaloid cocaine-X, X=F, Cl, Br, I. *Paripex A Indian Journal of Research* **2017**, *6,* 454-463.
5. Brandán, S.A. Understanding the potency of heroin against to morphine and cocaine. *International Journal of Science and Research Methodology* **2018**, *12*, 97-140.
6. Rudyk, R.A.; Checa, M.A.; Guzzetti, K.A.; Iramain, M.A.; Brandán, S.A. Behaviour of N-CH_3 Group in Tropane Alkaloids and correlations in their Properties. *International Journal of Science And Research Methodology* **2018**, *10,* 70-97.
7. Rudyk, R.A.; Checa, M.A.; Catalán, C.A.N.; Brandán, S.A. Structural, FT-IR, FT-Raman and ECD spectroscopic studies of free base, cationic and hydrobromide species of scopolamine alkaloid. *J. Mol. Struct*. **2019**, *1180*, 603-617. https://doi.org/10.1016/j.molstruc.2018.12.040.
8. Manzur, M.E.; Brandán, S.A. S(-) and R(+) Species Derived from Antihistaminic Promethazine Agent: Structural and Vibrational Studies. *Heliyon* **2019**, *5,* e02322, https://doi.org/10.1016/j.heliyon.2019.e02322.
9. Brandán, S.A. Structural and Vibrational Studies of Equilenin, Equilin and Estrone Steroids. *Biointerface Research in Applied Chemistry* **2019**, *9*, 4502-4516, https://doi.org/10.33263/BRIAC96.502516
10. M.A. Iramain, L. Davies, S.A. Brandán, FTIR, FT-Raman and UV-visible spectra of Potassium 3-furoyltrifluoroborate. *J. Mol. Struct.* **2018**, *1158*, 245-254, https://doi.org/10.1016/j.molstruc.2018.01.040.
11. Kausteklis, J.; Aleksa, V.; Iramain, M.A.; Brandán, S.A. Cation-anion interactions in 1-buthyl-3-methyl imidazolium nitrate ionic liquid and their effect on their structural and vibrational properties. *J Mol. Struct*. **2018**, *1164,* 1-14, https://doi.org/10.1016/j.molstruc.2018.03.100.
12. Iramain, M.A.; Davies, L.; Brandán, S.A. Evaluating structures, properties and vibrational and electronic spectra of the potassium 2-isonicotinoyltrifluoroborate salt. *J. Mol. Struct*. **2018**, *1163,* 41-53, https://doi.org/10.1016/j.molstruc.2018.02.098.
13. Kausteklis, J.; Aleksa, V.; Iramain, M.A.; Brandán, S.A. DFT study and vibrational assignment of 1-Butyl-3-methylimidazolium trifluoromethanesulfonate ionic liquid by using the FT-Raman spectrum. *J Mol. Struct.* **2019**, *1175*, 663-676, https://doi.org/10.1016/j.molstruc.2018.08.014.
14. Iramain, M.A.; Davies, L.; Brandán, S.A. Structural and spectroscopic differences among the Potassium 5-hydroxypentanoyltrifluoroborate salt and the furoyl and isonicotinoyl salts. *J Mol. Struct*. **2019**, *1176*, 718-728, https://doi.org/10.1016/j.molstruc.2019.02.010.
15. Iramain, M.A.; Ledesma, A.E.; Brandán, S.A. Structural properties and vibrational analysis of Potassium 5-Br-2-isonicotinoyltrifluoroborate salt. Effect of Br on the isonicotinoyl ring. *J Mol. Struct*. **2019**, 1184, 146-156, https://doi.org/10.1016/j.molstruc.2019.02.010.
16. Pulay, P.; Fogarasi, G.; Pongor, G.; Boggs, J.E.; Vargha, A. Combination of theoretical ab initio and experimental information to obtain reliable harmonic force constants. Scaled quantum mechanical (QM) force fields for glyoxal, acrolein, butadiene, formaldehyde, and ethylene. *J. Am. Chem. Soc*. **1983**, *105,* 7073, https://doi.org/10.1021/ja00362a005.
17. Rauhut, G.; Pulay, P. Transferable Scaling Factors for Density Functional Derived Vibrational Force Fields. *J. Phys. Chem*. **1995**, *99,* 3093-3100, https://doi.org/10.1021/j100010a019.

18. Sundius, T. Scaling of ab-initio force fields by MOLVIB. *Vib. Spectrosc*. **2002**, *29,* 89-95, https://doi.org/10.1016/S0924-2031(01)00189-8.
19. Dideberg, O.; Dupont, L. Crystal data on progesterone ($C_{21}H_{30}O_2$), desoxyeortieosterone ($C_{21}H_{30}O_3$), corticosterone ($C_{11}H_{30}O_4$) and aldosterone ($C_{21}H_{28}O_5H_20$). *J. Appl. Cryst.* **1971**, 4, 80-81, https://doi.org/10.1107/S0021889871006319.
20. Robel, P.; Baulieu, E-E. Dehydroepiandrosterone (DHEA) Is a Neuroactive Neurosteroid. *Annals New York Academy of sciences* **1995,** 82-110, https://doi.org/10.1111/j.1749-6632.1995.tb17374.x.
21. Sapolsky, R.M.; Romero, L.M.; Munck, A.U. How do glucocorticoids influence stress responses? Integrating permissive, suppressive, stimulatory, and preparative actions. *Endocr Rev* **2000**, *21*, 55–89, https://doi.org/10.1210/edrv.21.1.0389.
22. Singh, P.P.; Srivastava, H.K.; Pasha, F.A. DFT-based QSAR study of testosterone and its derivatives. *Bioorganic & Medicinal Chemistry* **2004**, *12,* 171–177, https://doi.org/10.1016/j.bmc.2003.11.002.
23. Boonstra, R.. Equipped for life: the adaptive role of the stress axis in male mammals. *J. Mamm.* **2005**, *86*, 236–247, https://doi.org/10.1644/BHE-001.1.
24. Szyczewski, A.; Pietrzak, J.; MÄobius, K. Structure of Free Radical in γ-Irradiated 21-Hydroxyprogesterone (Deoxycorticosterone) Single Crystals. ESR/ENDOR and DFT Studies. *Acta Physica Polonica* **2005**, *A108*, 119-126, https://doi.org/10.12693/APhysPolA.108.119.
25. Shikii, K.; Seki, H.; Sakamoto, S.; Sei, Y.; Utsumi, H. Yamaguchi, K. Intermolecular Hydrogen Bonding of Steroid Compounds: PFG NMR Diffusion Study, Cold-Spray Ionization (CSI)-MS and X-Ray Analysis. *Chem. Pharm. Bull*. **2005**, *53*, 792—795, https://doi.org/10.1248/cpb.53.792.
26. Bultinck, P.; Carbó-Dorca, R. Molecular quantum similarity using conceptual DFT descriptors. *J. Chem. Sci*. **2005**, *117,* 425–435, https://doi.org/10.1007/BF02708346.
27. Fetter, T.; Nunes, D.; Rodriguez, A.L.; da Silva Hoffmann, F.; Luz, C. Paiva, F.; Braga, F.A.; Campio, M.M.; Bauer, M.E. Relaxation and guided imagery program in patients with breast cancer undergoing radiotherapy is not associated with neuroimmunomodulatory effects. *J. of Psychosomatic Research* **2007**, 63647–655, https://doi.org/10.1016/j.jpsychores.2007.07.004.
28. Cherkasova, O.P.; Kargovsky, A.V.; Nazarov, M.M.; Smirnova, I.N.; Shkurinov, A.P. The effect of the nature of hydrogen bonding on THz and Raman spectra of cyclopentaphenanthrene derivatives. *IEEE* **2011**.
29. Yousuf, S.; Bibi, M.; Choudhary, M. I. 21-Hydroxypregna-1,4-diene-3,20-dione. *Acta Cryst*. **2011**, *E67,* o2122, https://doi.org/10.1107/S1600536811028674.
30. Sheriff, M.J.; Dantzer, B.; Delehanty, B.; Palme, R.; Boonstra, R. Measuring stress in wildlife: Techniques for quantifying glucocorticoids. *Oecol* **2011**, *166,* 869–887, https://doi.org/10.1007/s00442-011-1943-y.
31. Grinevich, V.; Seeburg, P.H.; Schwarz, M.K.; Jezova, D. Homer 1–a new player linking the hypothalamic-pituitary-adrenal axis activity to depression and anxiety. *Endocr Regul* **2012**, *46*, 153–159, https://doi.org/10.4149/endo_2012_03_153.
32. Baugh, A.T.; Oers, K.; van, Dingemanse, N.J.; Hau, M. Baseline and stress-induced glucocorticoid concentrations are not repeatable but covary within individual great tits (*Parus major*). *Gen Comp Endocrinol* **2014**, *208*, 154–163, https://doi.org/10.1016/j.ygcen.2014.08.014.
33. Minaeva, V.A. Minaev, B.F. Baryshnikov, G.V. Surovtsev, N.V. Cherkasova, O.P. Tkachenko, L.I. Karaush N.N., Stromylo, E.V. Temperature Effects in Low-Frequency Raman Spectra of Corticosteroid Hormones. *Optics and Spectroscopy* **2015**, *118,* 214–223, https://doi.org/10.1134/S0030400X15020149
34. Minaeva, V.A.; Cherkasova, O.P.; Minaev, B.F.; Baryshnikov, G.V.; Khmara, A.V. Features of Terahertz Adsorption and Raman Scattering of Mineralocorticoid Hormones. *Bulletin of the Russian Academy of Sciences. Physics* **2015**, *79*, 1196–1201, https://doi.org/10.3103/S1062873815010220.
35. Bauch, C.; Riechert, J.; Verhulst, S.; Becker, P.H. Telomere length reflects reproductive effort indicated by corticosterone levels in a long-lived seabird. *Mol Ecol* **2016**, *25,* 5785–5794, https://doi.org/10.1111/mec.13874.
36. Yang, X.; Xu, F.; Zhuang, C.; Bai, C.; Huang, W.; Song, M.; Han, Y.; Li, Y. Effects of Corticosterone on Immune Functions of Cultured Rat Splenic Lymphocytes Exposed to Aluminum Trichloride. *Biol Trace Elem Res* **2016**, *173*, 399–404, https://doi.org/10.1007/s12011-016-0678-3
37. Manickam, P.; Arizaleta, F.; Gurusamy, M.; Bhansali, S. Theoretical Studies of Cortisol-Imprinted Prepolymerization Mixtures: Structural Insights into Improving the Selectivity of Affinity Sensors. *J. Electrochemical Society* **2017**, *164*, B3077-B3080.
38. Vitousek, M.N.; Jenkins, B.R.; Hubbard, J.K.; Kaiser, S.A.; Safran, R.J. An experimental test of the effect of brood size on glucocorticoid responses, parental investment, and offspring phenotype. *Gen Comp Endocrinol* **2017**, *247*, 97–106, https://doi.org/10.1016/j.ygcen.2017.01.021.
39. Huang, X.F; Jiang, W.T; Liu, L.; Song, F.C; Zhu, X.; Shi, G.L; Ding, S.M; Ke, H.M; Wang, W.; O'Donnell, J.M.; Zhang, H-T; Luo, H.B; Wan, Y.Q; Song, G.Q; Xu, Y. A novel PDE9 inhibitor WYQ-C36D ameliorates corticosterone-induced neurotoxicity and depression-like behaviors by cGMP-CREB-related signaling. *CNS Neurosci Ther*. **2018**, *24*, 889–896, https://doi.org/10.1111/cns.12864.
40. Jimeno, B.; Hau, M.; Verhulst, S. Corticosterone levels reflect variation in metabolic rate, independent of 'stress. *Sci Rep.* **2018**, *8,* https://doi.org/10.1038/s41598-018-31258-z.
41. Reisinger, S.N.; Kong, E.; Molz, B.; Humberg, T.; Sideromenos, S.A.; Cicvaric, T.; Steinkellner, J..W.; Yang, M.; Cabatic, F.J.; Monje, H.H.; Sitte, B.J.; Nichols, D.D.; Pollak, Flotillin-1 interacts with the serotonin transporter and modulates chronic corticosterone response. *Genes, Brain and Behavior*. **2019**, *18*, e12482, https://doi.org/10.1111/gbb.12482.
42. Fair, M.; Vassoler, A.M.; Toorie, E.M. Byrnes, Transgenerational blunting of morphine-induced corticosterone secretion is associated with dysregulated gene expression in male offspring. *Brain Res.* **2018**, *15*, 19–25, https://doi.org/10.1016/j.brainres.2017.11.004.
43. Vera, F.; Antenucci, C.D.; Zenuto, R.R. Different regulation of cortisol and corticosterone in the subterranean rodent Ctenomys talarum: Responses to dexamethasone, angiotensin II, potassium, and diet, General and Comparative. *Endocrinology* **2019**, *27*, 108–117, https://doi.org/10.1016/j.ygcen.2018.05.019.
44. Xia, Q.; Wang, H.; Yin, H.; Yang, Z. Excessive corticosterone induces excitotoxicity of hippocampal neurons and sensitivity of potassium channels via insulin-signaling pathway. *Metabolic Brain Disease* **2019**, *34*, 119–128, https://doi.org/10.1007/s11011-018-0326-z.
45. Lee, C.; Yang, W.; Parr, R.G. Development of the Colle-Salvetti correlation-energy formula into a functional of the electron density. *Phys. Rev*. **1988**, *B37,* 785-789, https://doi.org/10.1103/PhysRevB.37.785.
46. Becke, A.D. Density-functional exchange-energy approximation with correct asymptotic behavior. *Phys. Rev*. **1988**, *A38*, 3098-3100, https://doi.org/10.1103/PhysRevA.38.3098.

47. Frisch, M.J.; Trucks, G.W.; Schlegel, H.B.; Scuseria, G.E.; Robb, M.A.; Cheeseman, J.R.; Scalmani, G.; Barone, V.; Mennucci, B.; Petersson, G.A.; Nakatsuji, H.; Caricato, M.; Li, X.; Hratchian, H.P.; Izmaylov, A.F.; Bloino, J.; Zheng, G.; Sonnenberg, J.L.; Hada, M.; Ehara, M.; Toyota, K.; Fukuda, R.; Hasegawa, J.; Ishida, M.; Nakajima, T.; Honda, Y.; Kitao, O.; Nakai, H.; Vreven, T.; Montgomery, J.A.; Peralta, J.E.; Ogliaro, F.; Bearpark, M.; Heyd, J.J.; Brothers, E.; Kudin, K.N.; Staroverov, V.N.; Kobayashi, R.; Normand, J.; Raghavachari, K.; Rendell, A.; Burant, J.C.; Iyengar, S.S.; Tomasi, J.; Cossi, M.; Rega, N.; Millam, J.M.; Klene, M.; Knox, J.E.; Cross, J.B.; Bakken, V.; Adamo, C.; Jaramillo, J.; Gomperts, R.; Stratmann, R.E.; Yazyev, O.; Austin, A.J.; Cammi, R.; Pomelli, C.; Ochterski, J.W.; Martin, R.L.; Morokuma, K.; Zakrzewski, V.G.; Voth, G.A.; Salvador, P.; Dannenberg, J.J.; Dapprich, S.; Daniels, A.D.; Farkas, O.; Foresman, J.B.; Ortiz, J.; Cioslowski, J.; Fox, D.J. Gaussian, Inc., Wallingford CT, **2009**.
48. Nielsen, A.B.; Holder, A.J. Gauss View 3.0. User's Reference, Gaussian Inc., Pittsburgh, PA, 2000–2003.
49. Miertus, S.; Scrocco, E.; Tomasi, J. Electrostatic interaction of a solute with a continuum. *Chem. Phys.* **1981**, *55*, 117–129, https://doi.org/10.1016/0301-0104(81)85090-2.
50. Tomasi, J.; Persico, J. Molecular Interactions in Solution: An Overview of Methods Based on Continous Distributions of the Solvent. *Chem. Rev.* **1994**, *94*, 2027-2094, https://doi.org/10.1021/cr00031a013.
51. Marenich, A.V.; Cramer, C.J.; Truhlar, D.G. Universal solvation model based on solute electron density and a continuum model of the solvent defined by the bulk dielectric constant and atomic surface tensions. *J. Phys. Chem.* **2009**, *B113*, 6378-6396, https://doi.org/10.1021/jp810292n.
52. Besler, B.H.; Merz, Jr. K.M.; Kollman, P.A. Atomic charges derived from semiempirical methods. *J. Comp. Chem.* **1990**, *11*, 431-439, https://doi.org/10.1002/jcc.540110404.
53. Glendening, E.; Badenhoop, J.K.; Reed, A.D.; Carpenter, J.E.; Weinhold, F. NBO 3.1; *Theoretical Chemistry Institute, University of Wisconsin; Madison,* WI, 1996.
54. Biegler-Köning, F.; Schönbohm, J.; Bayles, D. AIM2000; A Program to Analyze and Visualize Atoms in Molecules. *J. Comput. Chem.* **2001**, *22*, 545, http://dx.doi.org/10.1002/1096-987X(20010415)22:5%3C545::AID-JCC1027%3E3.0.CO;2-Y.
55. Ugliengo P. Moldraw Program, University of Torino, Dipartimento Chimica IFM, Torino, Italy, **1998**.
56. https://spectrabase.com/spectrum/
57. Keresztury, G.; Holly, S.; Besenyei, G.; Varga, J.; Wang, A.Y.; Durig, J.R. Vibrational spectra of monothiocarbamates-II. IR and Raman spectra, vibrational assignment, conformational analysis and ab initio calculations of **S**-methyl-N,N-dimethylthiocarbamate. *Spectrochim. Acta* **1993**, *49A,* 2007-2026, https://doi.org/10.1016/S0584-8539(09)91012-1.
58. Michalska D, Wysokinski. The prediction of Raman spectra of platinum(II) anticancer drugs by density functional theory. *Chemical Physics Letters* **2005**, *403*, 211-217, https://doi.org/10.1016/j.cplett.2004.12.096.
59. Paar, R.G.; Pearson, R.G. Absolute hardness: companion parameter to absolute electronegativity. *J. Am. Chem.* Soc. **1983**, *105*, 7512-7516, https://doi.org/10.1021/ja00364a005.
60. Minteguiaga, M.; Dellacassa, E.; Iramain, M.A.; Catalán, C.A.N.; Brandán, S.A. Synthesis, spectroscopic characterization and structural study of 2-isopropenyl-3-methylphenol, carquejiphenol, a carquejol derivative with potential medicinal use. *J Mol. Struct*. **2018**, *1165*, 332-343, https://doi.org/10.1016/j.molstruc.2018.04.001.
61. Ben M'leh, C.; Brandán, S.A.; Issaoui, N.; Roisnel, T.; Marouani, H. Synthesis, molecular structure, vibrational and theoretical studies of a new non-centrosymmetric organic sulphate with promising NLO properties. *J Mol. Struct.* **2018**, *1171*, 771-785, https://doi.org/10.1016/j.molstruc.2018.06.041
62. Gatfaoui, S.; Issaoui, N.; Brandán, S.A.; Roisnel, T.; Marouani, H. Synthesis and characterization of p-xylylenediaminiumbis(nitrate). Effects of the coordination modes of nitrate groups on their structural and vibrational properties. *Journal of Molecular Structure* **2018**, *1151*, 152-168, http://dx.doi.org/10.1016/j.molstruc.2017.09.027
63. Minteguiaga, M.; Dellacassa, E.; Iramain, M.A.; Catalán, C.A.N.; Brandán, S.A. FT-IR, FT-Raman, UV-Vis, NMR and structural studies of Carquejyl Acetate, a component of the essential oil from *Baccharis trimera* (Less.) DC. (Asteraceae). *J Mol. Struct*. **2019**, *1177*, 499-510, https://doi.org/10.1016/j.molstruc.2018.10.010.
64. Ruiz, H.J.; Neske, A.; Iramain, M.A.; Alvarez, P.E.; Leyton Bongiorno, P.; Brandán, S.A. FT-IR, FT-Raman and UV-visible spectra of motrilin acetogenin isolated from *Annona cherimolia. J Mol. Struct.* **2019**, 1196, 508-517, https://doi.org/10.1016/j.molstruc.2019.06.107
65. Trabelsi, S.; Issaoui, N.; Brandán, S.A.; Bardak, F.; Roisnel, T.; Atac , A.; Marouani, H. Synthesis and physic-chemical properties of a novel chromate compound with potential biological applications, bis(2-phenylethylammonium) chromate(VI). *J Mol. Struct.* **2019**, *1185,* 168-182, https://doi.org/10.1016/j.molstruc.2019.02.106.
66. Iramain, M.A.; Castillo, M.V.; Davies, L.; María E. Manzur, M.E.; Brandán, S.A. Structural and SQMFF study of potent insecticide 40,40-DDT combining the FT-IR and FT-Raman spectra with DFT calculations. *J. Mol. Struct.* **2020**, *1199,* 126964, https://doi.org/10.1016/j.molstruc.2019.126964.
67. Kausteklis, J.; Aleksa, V.; Iramain, M.A.; Brandán, S.A. DFT study and vibrational assignment of 1-Butyl-3-methylimidazolium trifluoromethanesulfonate ionic liquid by using the FT-Raman spectrum. *J. Mol. Struct.* **2019**, *1175,* 663-676, https://doi.org/10.1016/j.molstruc.2018.08.014.
68. Iramain, M.A.; Davies, L.; Brandán, S.A. Structural and spectroscopic differences among the Potassium 5-hydroxypentanoyltrifluoroborate salt and the furoyl and isonicotinoyl salts. *J Mol. Struct*. **2019**, *1176*, 718-728, https://doi.org/10.1016/j.molstruc.2019.02.010.
69. Veber, D.F.; Johnson, S.R.; Cheng, H-Y; Smith, B.R.; Ward, K.W.; Kopple, K.D. Molecular Properties That Influence the Oral Bioavailability of Drug Candidates. *J. Med. Chem*. **2002**, *45,* 2615-2623, https://doi.org/10.1021/jm020017n.
70. Bader, R.F.W. *Atoms in Molecules, A Quantum Theory.* Oxford University Press, Oxford, 1990.

6. ACKNOWLEDGEMENTS

This work was supported with grants from CIUNT Project Nº 26/D608 (Consejo de Investigaciones, Universidad Nacional de Tucumán, Argentina). The author would like to thank Prof. Tom Sundius for his permission to use MOLVIB.